13. C. Leduc, F. Ruhnow, J. Howard, S. Diez, *Proc. Natl. Acad. Sci. U.S.A.* **104**, 10847–10852 (2007).
14. K. J. Verhey, N. Kaul, V. Soppina, *Annu. Rev. Biophys.* **40**, 267–288 (2011).
15. H. Kim, T. Ha, *Rep. Prog. Phys.* **76**, 016601 (2013).
16. B. Huang, H. Babcock, X. Zhuang, *Cell* **143**, 1047–1058 (2010).
17. N. Fakhri, D. A. Tsyboulski, L. Cognet, R. B. Weisman, M. Pasquali, *Proc. Natl. Acad. Sci. U.S.A.* **106**, 14219–14223 (2009).
18. S. M. Bachilo *et al.*, *Science* **298**, 2361–2366 (2002).
19. D. A. Tsyboulski, S. M. Bachilo, R. B. Weisman, *Nano Lett.* **5**, 975–979 (2005).
20. R. B. Weisman, *Anal. Bioanal. Chem.* **396**, 1015–1023 (2010).
21. N. Fakhri, F. C. MacKintosh, B. Lounis, L. Cognet, M. Pasquali, *Science* **330**, 1804–1807 (2010).
22. S. Berciaud, L. Cognet, B. Lounis, *Phys. Rev. Lett.* **101**, 077402 (2008).
23. N. Hirokawa, Y. Noda, Y. Tanaka, S. Niwa, *Nat. Rev. Mol. Cell Biol.* **10**, 682–696 (2009).
24. G. V. Los *et al.*, *ACS Chem. Biol.* **3**, 373–382 (2008).
25. C. P. Brangwynne, G. H. Koenderink, F. C. Mackintosh, D. A. Weitz, *Phys. Rev. Lett.* **100**, 118104 (2008).
26. I. M. Kulic *et al.*, *Proc. Natl. Acad. Sci. U.S.A.* **105**, 10011–10016 (2008).
27. K. Jaqaman *et al.*, *Nat. Methods* **5**, 695–702 (2008).
28. D. Cai, D. P. McEwen, J. R. Martens, E. Meyhofer, K. J. Verhey, *PLOS Biol.* **7**, e1000216 (2009).
29. S. Courty, C. Luccardini, Y. Bellaiche, G. Cappello, M. Dahan, *Nano Lett.* **6**, 1491–1495 (2006).
30. S. Dunn *et al.*, *J. Cell Sci.* **121**, 1085–1095 (2008).
31. Š. Bálint, I. Verdeny Vilanova, Á. Sandoval Álvarez, M. Lakadamyali, *Proc. Natl. Acad. Sci. U.S.A.* **110**, 3375–3380 (2013).
32. C. P. Brangwynne *et al.*, *J. Cell Biol.* **173**, 733–741 (2006).
33. M. Rubinstein, R. Colby, *Polymer Physics (Chemistry)* (Oxford Univ. Press, New York, 2003).
34. B. Fabry *et al.*, *Phys. Rev. Lett.* **87**, 148102 (2001).
35. A. W. C. Lau, B. D. Hoffman, A. Davies, J. C. Crocker, T. C. Lubensky, *Phys. Rev. Lett.* **91**, 198101 (2003).
36. A. J. Levine, F. C. MacKintosh, *J. Phys. Chem. B* **113**, 3820–3830 (2009).
37. This behavior can be understood as follows: The low-frequency behavior, corresponding to times longer than $\tau_c$, is white noise that is independent of frequency, characteristic of uncorrelated fluctuations. For times shorter than $\tau_c$, by contrast, the binding of myosins, subsequent force generation, and eventual release combine to result in a random walk of the net force due to multiple motors in time, with $\langle \Delta f^2(\tau) \rangle \propto \tau$, the Fourier transform of which is $\langle f^2 \rangle_\omega \propto 1/\omega^2$.
38. B. Ramamurthy, C. M. Yengo, A. F. Straight, T. J. Mitchison, H. L. Sweeney, *Biochemistry* **43**, 14832–14839 (2004).
39. A. F. Straight *et al.*, *Science* **299**, 1743–1747 (2003).
40. M. Kovács, J. Tóth, C. Hetényi, A. Málnási-Csizmadia, J. R. Sellers, *J. Biol. Chem.* **279**, 35557–35563 (2004).

### ACKNOWLEDGMENTS

We thank L. Cognet, J. Enderlein, M. Guo, J. Lippincott-Schwartz, and D. A. Weitz for helpful discussions; I. Schaap and M. Platen for atomic force microscopy measurements; and the Kavli Institute for Theoretical Physics (University of California, Santa Barbara) for hospitality and useful discussions. Supported by the Center for Nanoscale Microscopy and Molecular Physiology of the Brain and the Collaborative Research Center SFB 937 (Project A2), both funded by the Deutsche Forschungsgemeinschaft, as well as by the Foundation for Fundamental Research on Matter of the Netherlands Organization for Scientific Research, Welch Foundation grant C-1668, and NSF grant NSF PHY11-25915. N.F. was supported by a Human Frontier Science Program Fellowship. N.F. and C.F.S. are inventors on a provisional U.S. patent application on the method used in the paper, filed by Georg-August-Universität. The single-walled carbon nanotubes are available from M.P. under a material transfer agreement with Rice University.

### SUPPLEMENTARY MATERIALS

www.sciencemag.org/content/344/6187/1031/suppl/DC1
Materials and Methods
Figs. S1 to S14
Movies S1 to S4
References (*41*–*45*)

24 December 2013; accepted 2 May 2014
10.1126/science.1250170

STRUCTURAL BIOLOGY

# Structures of PI4KIIIβ complexes show simultaneous recruitment of Rab11 and its effectors

**John E. Burke,[1]*† Alison J. Inglis,[1] Olga Perisic,[1] Glenn R. Masson,[1] Stephen H. McLaughlin,[1] Florentine Rutaganira,[2] Kevan M. Shokat,[2] Roger L. Williams[1]***

**Phosphatidylinositol 4-kinases (PI4Ks) and small guanosine triphosphatases (GTPases) are essential for processes that require expansion and remodeling of phosphatidylinositol 4-phosphate (PI4P)–containing membranes, including cytokinesis, intracellular development of malarial pathogens, and replication of a wide range of RNA viruses. However, the structural basis for coordination of PI4K, GTPases, and their effectors is unknown. Here, we describe structures of PI4Kβ (PI4KIIIβ) bound to the small GTPase Rab11a without and with the Rab11 effector protein FIP3. The Rab11-PI4KIIIβ interface is distinct compared with known structures of Rab complexes and does not involve switch regions used by GTPase effectors. Our data provide a mechanism for how PI4KIIIβ coordinates Rab11 and its effectors on PI4P-enriched membranes and also provide strategies for the design of specific inhibitors that could potentially target plasmodial PI4KIIIβ to combat malaria.**

Intracellular compartments are essential to eukaryotic cell biology, and both small guanosine triphosphatases (GTPases) and lipids such as phosphoinositides are key components of compartment identity (*1*, *2*). The phosphatidylinositol 4-kinases (PI4Ks) and the small G-protein Rab11 play prominent roles in compartment identity. PI4KIIIβ is one of four mammalian PI4K enzymes that phosphorylate phosphatidylinositol to generate phosphatidylinositol 4-phosphate (PI4P). PI4KIIIβ localizes primarily at the Golgi and is essential for Golgi formation and function (*3*–*5*). PI4P is recognized by protein modules, including the PH domains of oxysterol-binding protein, ceramide transfer protein, and four-phosphate-adaptor protein, that are important for intra-Golgi transport (*6*–*8*). However, typically, lipid recognition alone is not sufficient for Golgi localization, which requires both PI4P and specific small GTPases. In addition to its catalytic role in synthesizing PI4P, PI4KIIIβ also has noncatalytic roles that rely on the interactions with other proteins such as the small GTPase Rab11 (*9*). Rab11 is predominately located on recycling endosomes (*10*). However, Rab11 is also found associated with Golgi membranes, which requires an interaction with PI4KIIIβ (*9*).

PI4KIIIβ activity is essential for replication of a range of RNA viruses, including enteroviruses, SARS coronavirus, and hepatitis C virus (*11*, *12*). These RNA viruses hijack the activity of host cell PI4KIIIβ to generate replication organelles enriched in PI4P. There is no approved antiviral therapy for enteroviruses. However, several compounds inhibit enteroviral replication by targeting cellular PI4KIIIβ (*13*, *14*). PI4KIIIβ is also important in malaria, and inhibitors of *Plasmodium falciparum* PI4KIIIβ are potent antimalarial agents. However, mutations in both PI4KIIIβ and Rab11 confer resistance to these compounds (*15*). Inhibition of *P. falciparum* PI4KIIIβ prevents the membrane ingression that occurs during completion of the asexual erythrocytic stage of the plasmodial life cycle. The role of *Plasmodium* Rab11 and PI4KIIIβ in membrane remodeling is similar to the role of Rab11 and PI4KIIIβ in cytokinesis in *Drosophila* spermatocytes (*16*). In *Drosophila*, PI4KIIIβ is required for the recruitment of both Rab11 and its downstream effectors.

To understand how PI4KIIIβ can both recruit Rab11 and enable its interactions with Rab11 effectors, we used hydrogen-deuterium exchange mass spectrometry (HDX-MS) to facilitate the x-ray crystal structure of human PI4KIIIβ in complex with Rab11a–GTPγS [GTPγS, guanosine 5′-*O*-(3′-thiotriphosphate)] at 2.9 Å resolution (see supplementary materials and methods). To form crystals, highly flexible regions of PI4KIIIβ identified by HDX-MS were truncated (residues 1 to 120, 408 to 507, and 785 to 801) (Fig. 1A). This included a C-terminal region necessary for catalytic activity (fig. S2A). The PI4KIIIβ structure consists of two domains, a right-handed helical solenoid (residues 128 to 243) and a kinase domain (residues 306 to 801) (Fig. 1B), that are related to the PI3Ks (fig. S3). The kinase domain has two lobes, an N-terminal lobe dominated by a five-stranded antiparallel β sheet and a C-terminal lobe that is largely helical, with the adenosine triphosphate (ATP)–binding site located in a cleft between the lobes. The N lobe of PI4KIIIβ has a PI4KIIIβ-distinct, large insertion (residues 391 to 539) (Fig. 1B).

[1]Medical Research Council (MRC) Laboratory of Molecular Biology, Cambridge CB2 0QH, UK. [2]Howard Hughes Medical Institute and Department of Cellular and Molecular Pharmacology, University of California, San Francisco (UCSF), San Francisco, CA 94158, USA.
***Corresponding author. E-mail: jeburke@uvic.ca (J.E.B.); rlw@mrc-lmb.cam.ac.uk (R.L.W.)** †Present address: Department of Biochemistry and Microbiology, University of Victoria, Victoria, British Columbia, Canada.

PI4KIIIβ makes a distinct interaction with Rab11a that is not characteristic of any Rab or Arf effector (*17*). This interaction involves primarily helix α3 of the PI4KIIIβ helical domain (Figs. 1B and 2A). Because a previous study of human PI4KIIIβ mapped the epitope interacting with Rab11a to the insertion in the N lobe of the kinase domain (*9*), we also used HDX-MS to determine the Rab11 binding site on full-length PI4KIIIβ in solution (figs. S4 and S5). The HDX-MS measurements confirmed the interaction between the N-terminal part of the PI4KIIIβ helical domain and Rab11a (fig. S5). Soluble Rab11 had no effect on PI4KIIIβ activity (fig. S2B).

The PI4KIIIβ-Rab11 interface is predominantly hydrophobic, with no hydrogen bonds or salt links (Fig. 2A). Surprisingly, PI4KIIIβ makes only a single, peripheral contact with the Rab11 switch I (only with the edge residues 38-LES-40 of switch I) and no contact with switch II (Fig. 2, A and B). The switch regions change conformation depending on whether Rab11 is bound to GTP or guanosine diphosphate (GDP). Consistent with the structure, PI4KIIIβ bound both GTP- and GDP-loaded Rab11, with a slight preference for GTP (Fig. 2D and fig. S6). Within the PI4KIIIβ-Rab11 interface, G155 (*18*) of PI4KIIIβ makes a direct contact with the ribose moiety of GTPγS bound to the Rab11 (Fig. 2A). The small residue at position 155 is completely conserved among PI4KIIIβ homologs, from yeast to mammals, and might be required to maintain the contact with Rab11. Indeed, a PI4KIIIβ-G155D mutation (where G155D denotes $Gly^{155}$→$Asp^{155}$) decreased binding to Rab11 (Fig. 2, C and D). Consistent with PI4KIIIβ directly contacting the nucleotide, PI4KIIIβ decreased the rate of EDTA-mediated Rab11 nucleotide exchange (fig. S2C). PI4KIIIβ residues Y159, N162, and F165 also form prominent contacts with the Rab11. The mutants PI4KIIIβ-Y159A, N162A, and F165A and the double mutant Y159A/N162A all eliminated measurable binding to Rab11 (Fig. 2, C and D). The Rab11 residues interacting with PI4KIIIβ are all conserved among Rab11a and Rab11b, but not among other Rabs that do not bind PI4KIIIβ (Fig. 2B). The PI4KIIIβ residues interacting with Rab11 are also strongly conserved among PI4KIIIβ orthologs (Fig. 2B and fig. S3).

The structure of the PI4KIIIβ-Rab11a complex shows that the Rab11a switch regions remained available to contact Rab11a effectors. Among the Rab11 effectors is a family of related proteins known as the Rab11 family-interacting proteins, or FIPs (*19*). In *Drosophila*, both catalytic and noncatalytic functions of Four wheel drive (PI4KIIIβ ortholog in *Drosophila*) are required for the proper localization of both Rab11a and its downstream effector Nuf (ortholog of human FIP3) at the cleavage furrow, which is essential for cytokinesis in spermatocytes (*16*). During interphase, FIP3 is required for the structural integrity of the pericentriolar recycling endosome compartment (*20*), whereas during cytokinesis, it is involved in delivering material from recycling endosomes to the cleavage furrow (*21*). The FIP proteins interact with Rab11 using a conserved C-terminal region known as the Rab-binding domain (RBD). Two FIPs form a parallel coiled-coil dimer with two Rab11 binding sites (*22*–*24*) that engage both switch I and switch II of Rab11.

The structure of Rab11a bound to the RBD domain of FIP3 (*22*–*24*) and our structure of the PI4KIIIβ-Rab11a complex suggest that a ternary complex might be formed. Glutathione *S*-transferase (GST) pulldowns carried out with the GST-tagged RBD domain from FIP3 (residues 713 to 756) revealed that the complex of the FIP3-RBD with GTPγS-loaded Rab11a (Q70L) was able to bind PI4KIIIβ (Fig. 3A). To understand how this occurs, we crystallized a ternary PI4KIIIβ/Rab11a/FIP3-RBD complex. Although this is a low-resolution (6 Å) structure with a very large asymmetric unit (~1 MD, containing 12 ternary complexes), both FIP3 and PI4KIIIβ were bound simultaneously to Rab11a–GTPγS (Fig. 3B and fig. S7). The ability of PI4KIIIβ to recruit both Rab11a and its downstream effectors is unlikely to be limited to only the FIP family of proteins. The production of PI4P by Pik1, the yeast ortholog of PI4KIIIβ, is required for the Ypt32 (yeast ortholog of Rab11)–dependent recruitment of the Rab guanine nucleotide exchange factor Sec2p (*25*), in a phosphoinositide-dependent regulation of Rab activation cascade. The conservation of the PI4KIIIβ-Rab11a interface in Pik1 and Ypt32 indicates the possibility of a ternary Pik1-Ypt32-Sec2 complex. Furthermore, the switch-independent interaction of PI4KIIIβ with Rab11 suggests that ternary PI4KIIIβ/Rab11/RabGAP and PI4KIIIβ/Rab11/Rab Escort complexes could also be formed (fig. S8).

The inhibitor PIK93 shows a clear selectivity for PI4KIIIβ over PI4KIIIα, with partial selectivity over PI3Ks (*26*). This inhibitor has been used to decipher PI4K-specific functions (*27*), for example, in demonstrating the role of PI4KIIIβ in viral replication (*11*). PIK93 bound in the ATP-binding pocket, using its thiazol and acetamide moieties to make a pair of hydrogen bonds with the backbone of V598 in the hinge between the N and C lobes (Fig. 4A and fig. S9A). The PI4KIIIβ ATP-binding pocket and those of PI3Ks and

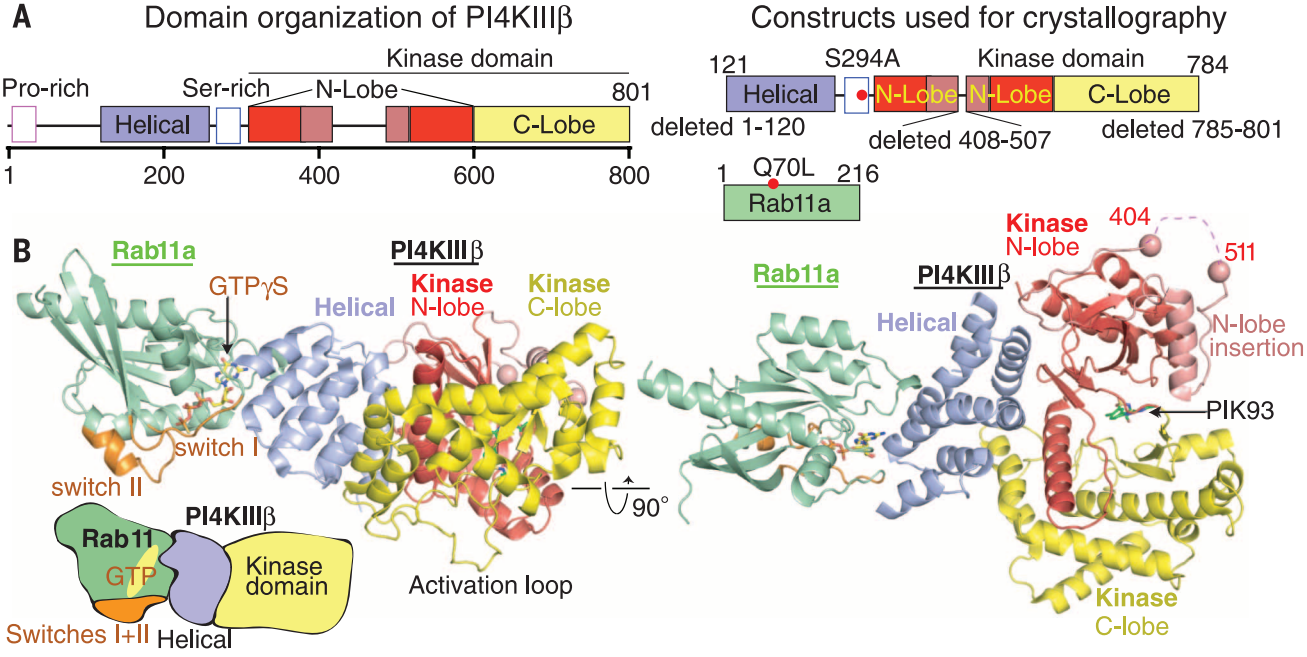


**Fig. 1. Crystal structure of the human PI4KIIIβ complex with Rab11a (Q70L)–GTPγS.** (**A**) Full-length PI4KIIIβ (isoform 2) (left) and constructs of PI4KIIIβ and Rab11a (Q70L) used for crystallization (right). The PI4KIIIβ crystallization construct contained three deletions, as well as an S294A mutation. (**B**) Overall architecture of the complex. The PI4K-specific insertion (residues 391 to 540) in the N lobe is salmon colored. The large spheres mark a disordered region within which residues 408 to 507 are deleted. The switch I and switch II regions of Rab11a (Q70L) are represented in orange.

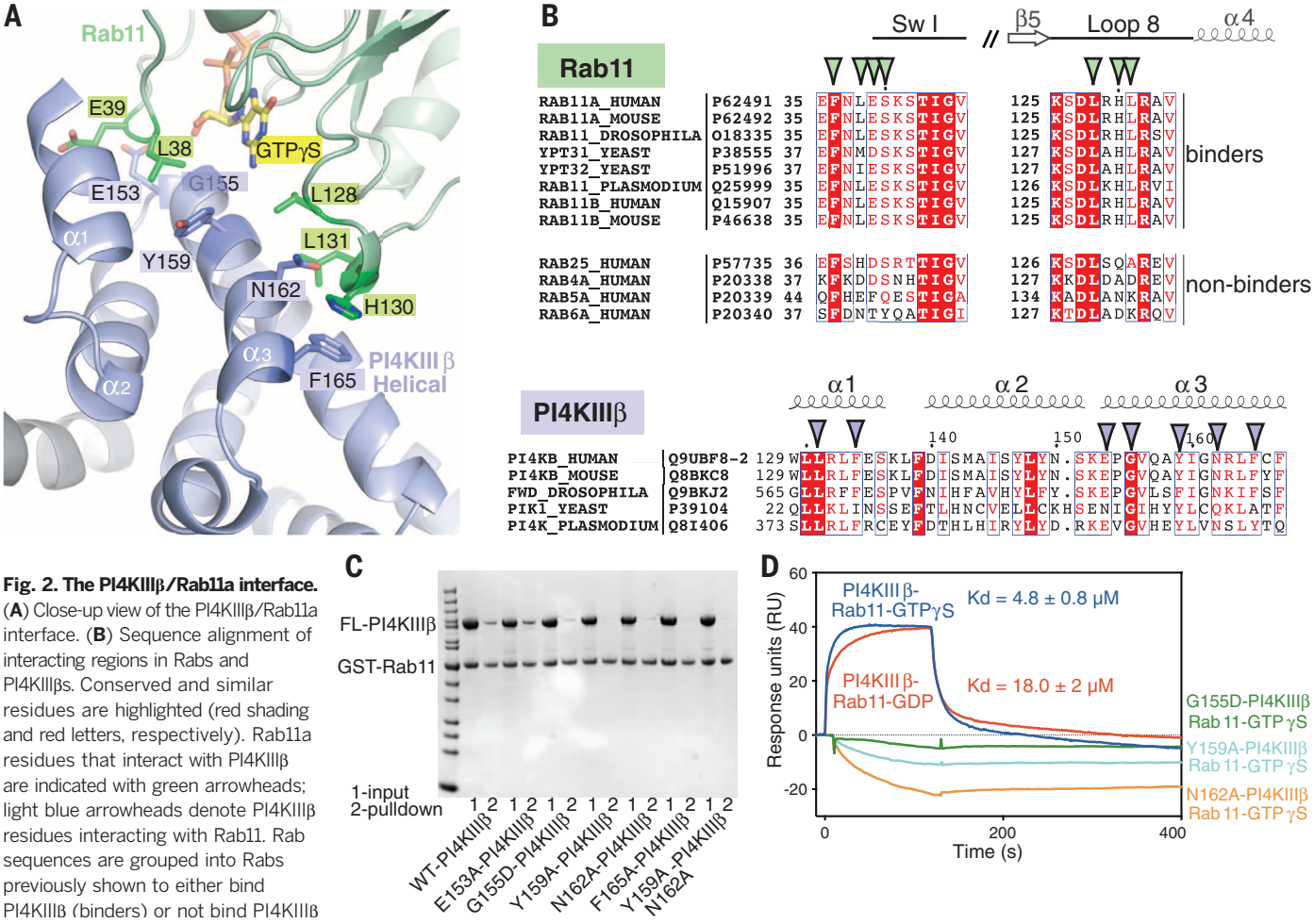


**Fig. 2. The PI4KIIIβ/Rab11a interface.** (**A**) Close-up view of the PI4KIIIβ/Rab11a interface. (**B**) Sequence alignment of interacting regions in Rabs and PI4KIIIβs. Conserved and similar residues are highlighted (red shading and red letters, respectively). Rab11a residues that interact with PI4KIIIβ are indicated with green arrowheads; light blue arrowheads denote PI4KIIIβ residues interacting with Rab11. Rab sequences are grouped into Rabs previously shown to either bind PI4KIIIβ (binders) or not bind PI4KIIIβ (nonbinders). (**C**) Pull-down assays with GST-tagged Rab11A (Q70L)–GTPγS and either wild-type or mutant full-length PI4KIIIβ. The inputs and the bound proteins (lanes 1 and 2, respectively) were analyzed on SDS gels stained with InstantBlue. (**D**) Surface plasmon resonance (SPR) analysis of the full-length wild-type PI4KIIIβ binding to the immobilized GST-tagged Rab11a (Q70L) loaded with either GDP (red sensogram) or GTPγS (blue). The affinity of PI4KIIIβ for GST-Rab11a is indicated next to the graphs (data are mean ± SEM based on five independent experiments). Full details are shown in fig. S6. Also shown are the sensograms for several PI4KIIIβ mutants binding to Rab11a (Q70L)–GTPγS.

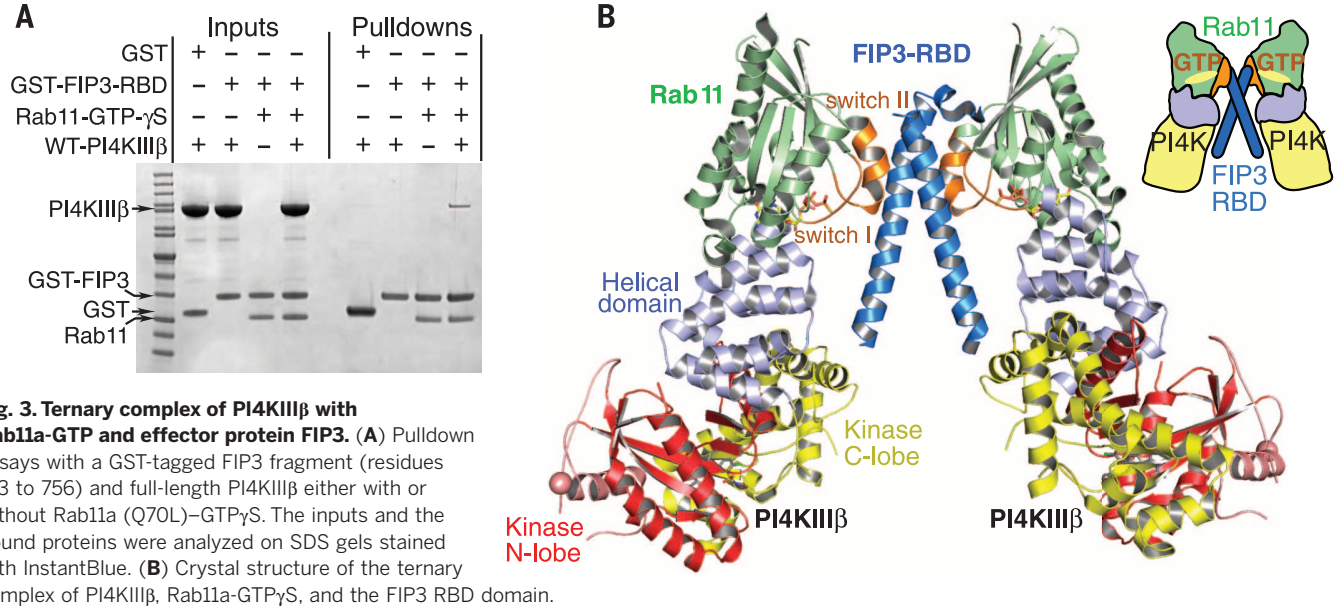


**Fig. 3. Ternary complex of PI4KIIIβ with Rab11a-GTP and effector protein FIP3.** (**A**) Pulldown assays with a GST-tagged FIP3 fragment (residues 713 to 756) and full-length PI4KIIIβ either with or without Rab11a (Q70L)–GTPγS. The inputs and the bound proteins were analyzed on SDS gels stained with InstantBlue. (**B**) Crystal structure of the ternary complex of PI4KIIIβ, Rab11a-GTPγS, and the FIP3 RBD domain.

phosphatidylinositol 3-kinase–related kinases show considerable consistency. Most of the contacts that PIK93 makes with PI4KIIIβ involve residues that are conserved among both the PI3Ks and PI4Ks (Fig. 4, A and C). The PIK93 sulfamoyl moiety makes a hydrogen bond with K549 of PI4KIIIβ. Although this lysine is conserved in the PI3Ks, its conformation is variable, and in the structures of PIK93 in complex with either p110γ (*26*) or Vps34 (*28*), the equivalent lysine does not make this hydrogen bond (fig. S9B). There is more sequence divergence in the residues near the hinge. Though the class III PI3K Vps34 is more closely related to PI4KIIIβ than other PI3Ks, PIK93 is a poor inhibitor of Vps34. The PI4KIIIβ has a great deal of space near the hinge that allows PIK93 to form hydrogen bonds with the hinge and simultaneously optimize contacts elsewhere (fig. S9B). Y583 packs against the hinge to form one wall of the pocket contacting both the Cl substituent of the thiazole and the phenyl moiety. The structure helps rationalize why a Y583M mutation makes PI4KIIIβ insensitive to wortmannin and PIK93 (*29*) (fig. S9C).

Inhibitors specific against plasmodial PI4KIIIβ are potent antimalarial agents, and resistance mutations in either Rab11a or PI4KIIIβ can evade the antimalarial activity of these compounds (*15*). The plasmodial Y1356F resistance mutation involves the hinge residue, which is equivalent to human P597. It may be that Y1356 makes an additional interaction with the inhibitor (Fig. 4, B and D). The S1320L resistance mutation corresponds to F561 in human PI4KIIIβ. This residue packs against Y583 (Y1342 in *P. falciparum*), which forms one wall of the inhibitor-binding pocket, and the mutation may alter the conformation of the pocket. The third mutation, H1484Y, is in a bend between kα8 and kα9 and is equivalent to H728 in human PI4KIIIβ. Several somatic mutations associated with cancer have been detected for human p110α PI3K in the equivalent bend, and the most common of these mutations increases enzymatic activity and membrane binding (*30*). It is plausible that the H1484Y resistance mutation is making PI4KIIIβ more active.

The structures of a binary complex of PI4KIIIβ with Rab11a and a ternary complex of PI4KIIIβ with Rab11a and Rab11-effector FIP3 revealed a Rab11 interface that is compatible with the PI4KIIIβ-driven recruitment of Rab11 and its effectors to PI4P-enriched membranes. PI4KIIIβ plays key roles in regulating Rab11a in cytokinesis of spermatocytes, recruitment of Rab guanine nucleotide exchange factors in yeast, and membrane remodeling in *Plasmodium* development. The PI4KIIIβ-Rab11 interface is conserved and demonstrates that PI4K, in addition to its kinase activity, plays key kinase-independent roles in mediating these membrane-trafficking events. This structure opens up exciting prospects for the development of highly specific inhibitors, which may act as potent antimalarial and antiviral therapeutics.

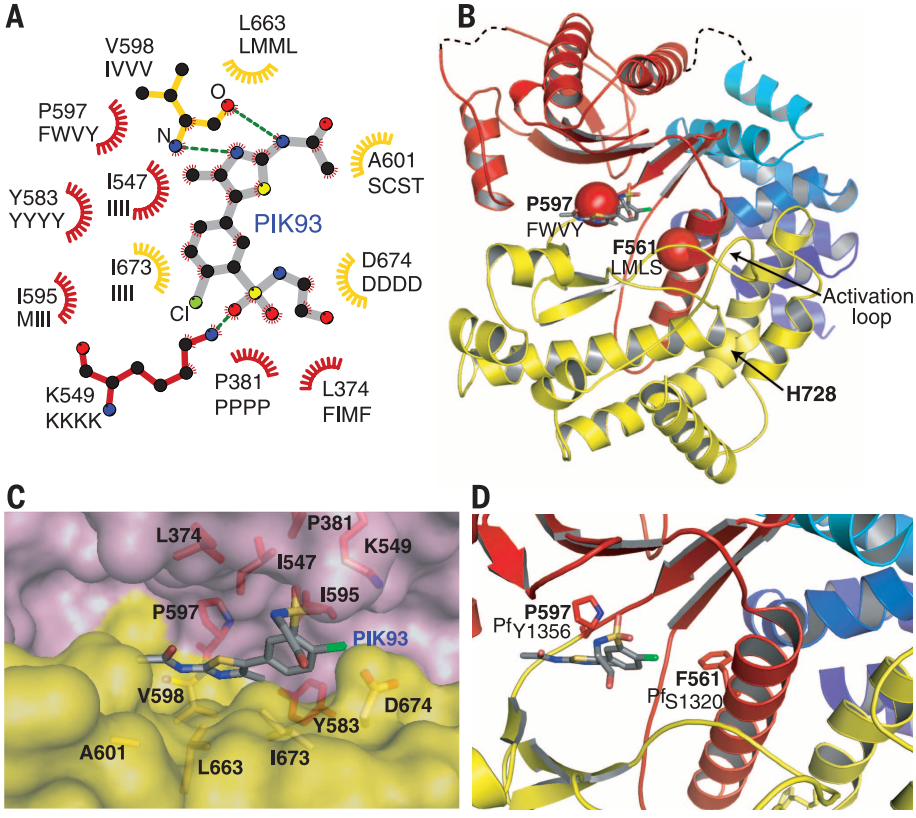


**Fig. 4. Inhibitor binding to PI4KIIIβ.** (**A**) Interactions of PI4KIIIβ with PIK93. Dotted lines represent putative hydrogen bonds [prepared by LIGPLOT (*31*)]. For each PI4KIIIβ residue, the equivalent residues are shown below for human Vps34, human mTOR, human p110α, and *P. falciparum* PI4KIIIβ (left to right). (**B**) Ribbon diagram of PI4KIIIβ, illustrating sites of *P. falciparum* resistance mutations (spheres). The helical domain is colored from dark to light blue from N terminus to the C terminus. (**C**) PIK93 bound to PI4KIIIβ. (**D**) Close-up of the active site, illustrating positions of *P. falciparum* resistance mutations.


## REFERENCES AND NOTES

1. S. Jean, A. A. Kiger, *Nat. Rev. Mol. Cell Biol.* **13**, 463–470 (2012).
2. F. H. Santiago-Tirado, A. Bretscher, *Trends Cell Biol.* **21**, 515–525 (2011).
3. A. Godi *et al.*, *Nat. Cell Biol.* **1**, 280–287 (1999).
4. A. Audhya, M. Foti, S. D. Emr, *Mol. Biol. Cell* **11**, 2673–2689 (2000).
5. V. A. Sciorra *et al.*, *Mol. Biol. Cell* **16**, 776–793 (2005).
6. T. P. Levine, S. Munro, *Curr. Biol.* **12**, 695–704 (2002).
7. S. Dowler *et al.*, *Biochem. J.* **351**, 19–31 (2000).
8. G. D'Angelo *et al.*, *Nature* **501**, 116–120 (2013).
9. P. de Graaf *et al.*, *Mol. Biol. Cell* **15**, 2038–2047 (2004).
10. O. Ullrich, S. Reinsch, S. Urbé, M. Zerial, R. G. Parton, *J. Cell Biol.* **135**, 913–924 (1996).
11. N.-Y. Hsu *et al.*, *Cell* **141**, 799–811 (2010).
12. N. Altan-Bonnet, T. Balla, *Trends Biochem. Sci.* **37**, 293–302 (2012).
13. H. M. van der Schaar *et al.*, *Antimicrob. Agents Chemother.* **57**, 4971–4981 (2013).
14. M. Arita *et al.*, *J. Virol.* **85**, 2364–2372 (2011).
15. C. W. McNamara *et al.*, *Nature* **504**, 248–253 (2013).
16. G. Polevoy *et al.*, *J. Cell Biol.* **187**, 847–858 (2009).
17. A. R. Khan, J. Ménétrey, *Structure* **21**, 1284–1297 (2013).
18. Single-letter abbreviations for the amino acid residues are as follows: A, Ala; C, Cys; D, Asp; E, Glu; F, Phe; G, Gly; H, His; I, Ile; K, Lys; L, Leu; M, Met; N, Asn; P, Pro; Q, Gln; R, Arg; S, Ser; T, Thr; V, Val; W, Trp; and Y, Tyr.
19. E. E. Kelly, C. P. Horgan, M. W. McCaffrey, *Biochem. Soc. Trans.* **40**, 1360–1367 (2012).
20. C. P. Horgan *et al.*, *Traffic* **8**, 414–430 (2007).
21. G. M. Wilson *et al.*, *Mol. Biol. Cell* **16**, 849–860 (2005).
22. S. Eathiraj, A. Mishra, R. Prekeris, D. G. Lambright, *J. Mol. Biol.* **364**, 121–135 (2006).
23. W. N. Jagoe *et al.*, *Structure* **14**, 1273–1283 (2006).
24. T. Shiba *et al.*, *Proc. Natl. Acad. Sci. U.S.A.* **103**, 15416–15421 (2006).
25. E. Mizuno-Yamasaki, M. Medkova, J. Coleman, P. Novick, *Dev. Cell* **18**, 828–840 (2010).
26. Z. A. Knight *et al.*, *Cell* **125**, 733–747 (2006).
27. B. Tóth *et al.*, *J. Biol. Chem.* **281**, 36369–36377 (2006).
28. S. Miller *et al.*, *Science* **327**, 1638–1642 (2010).
29. A. Balla *et al.*, *Biochemistry* **47**, 1599–1607 (2008).
30. J. E. Burke, O. Perisic, G. R. Masson, O. Vadas, R. L. Williams, *Proc. Natl. Acad. Sci. U.S.A.* **109**, 15259–15264 (2012).
31. R. A. Laskowski, M. B. Swindells, *J. Chem. Inf. Model.* **51**, 2778–2786 (2011).



## ACKNOWLEDGMENTS

We thank C. Mueller-Dieckmann and D. De Sanctis at the European Synchrotron Radiation Facility and C. Lobley at Diamond Light Source for assistance with beamlines ID23-EH2, ID29, and I04-1; S. Maslen, M. Skehel, and S. Y. Peak-Chew for help with HDX-MS setup; and M. Yu for help with x-ray data collection. J.E.B. was supported by a grant from the British Heart Foundation (PG11/109/29247) and F. Rutaganira by an NSF predoctoral fellowship. This work was funded by the NIH (RO1AI099245 to K.M.S.) and the UK MRC (MC_U105184308 to R.L.W). K.M.S. has filed for patent protection on PIK93 analogs in the following application between UCSF and Stanford University: PCT/US2012/059023. Coordinates and structure factors have been deposited in the Protein Data Bank with accession numbers 4D0L and 4D0M, for PI4KIIIβ/Rab11a and PI4KIIIβ/Rab11a/FIP3 complexes, respectively. Author contributions: J.E.B., O.P., and R.L.W. initiated the project and designed the experiments; J.E.B., A.J.I., G.R.M., and O.P. performed the experiments; J.E.B. and R.L.W. carried out the structure determination and analysis; S.H.M. performed SPR analysis; F.R. and K.M.S. synthesized PI4K inhibitors; and J.E.B., O.P., and R.L.W. wrote the manuscript.


## SUPPLEMENTARY MATERIALS

www.sciencemag.org/content/344/6187/1035/suppl/DC1
Materials and Methods
Figs. S1 to S9
Table S1
References (*32*–*42*)

14 March 2014; accepted 30 April 2014
10.1126/science.1253397

Science

# Structures of PI4KIIIβ complexes show simultaneous recruitment of Rab11 and its effectors

John E. Burke, Alison J. Inglis, Olga Perisic, Glenn R. Masson, Stephen H. McLaughlin, Florentine Rutaganira, Kevan M. Shokat and Roger L. Williams

*Science* **344** (6187), 1035-1038.
DOI: 10.1126/science.1253397

**How to recruit membrane trafficking machinery**

PI4KIIIβ is a lipid kinase that underlies Golgi function and is enlisted in biological responses that require rapid delivery of membrane vesicles, such as during the extensive membrane remodeling that occurs at the end of cell division. Burke *et al.* determined the structure of PI4KIIIβ in a complex with the membrane trafficking GTPase Rab11a. The way in which the proteins interact gives PI4KIII β the ability to simultaneously recruit Rab11a and its effectors on specific membranes.

*Science*, this issue p. 1035